ADVANCED ENERGY MATERIALS

www.advenergymat.de

Triboelectrification-Enabled Self-Charging Lithium-Ion Batteries

Kun Zhao, Ya Yang, Xi Liu, and Zhong Lin Wang**

Li-ion batteries as energy storage devices need to be periodically charged for sustainably powering electronic devices owing to their limited capacities. Here, the feasibility of utilizing Li-ion batteries as both the energy storage and scavenging units is demonstrated. Flexible Li-ion batteries fabricated from electrospun $LiMn_2O_4$ nanowires as cathode and carbon nanowires as anode enable a capacity retention of 90% coulombic efficiency after 50 cycles. Through the coupling between triboelectrification and electrostatic induction, the adjacent electrodes of two Li-ion batteries can deliver an output peak voltage of about 200 V and an output peak current of about 25 μA under ambient wind-induced vibrations of a hexafluoropropene–tetrafluoroethylene copolymer film between the two Li-ion batteries. The self-charging Li-ion batteries have been demonstrated to charge themselves up to 3.5 V in about 3 min under wind-induced mechanical excitations. The advantages of the self-charging Li-ion batteries can provide important applications for sustainably powering electronics and self-powered sensor systems.

Energy storage and conversion are two most crucial technologies in today's renewable energy systems, which can be achieved by usually two different and independent devices.[1,2] As for energy storage devices, Li-ion battery is one of the most effective devices that can convert electric energy into chemical energy through driving Li ions to move between the anode and cathode for accomplishing the electrochemical reactions.[3–6] As for energy conversion, various energy scavenging devices have been exploited to convert ambient energies such as solar, thermal, mechanical energies into electricity.[7–10] Among them, a nanogenerator based on piezoelectric effect or triboelectric effect is one of the effective energy harvesting devices to scavenge mechanical energy.[11–13] Especially, triboelectric effect has been extensively utilized to fabricate devices for scavenging almost all forms of mechanical energies.[14–16] Due to limited capacities, Li-ion batteries require to be periodically charged for sustainably powering electronic devices. To solve the sustainable charging issues of Li-ion batteries, an ideal solution may be to utilize the Li-ion batteries as a power generator so that the invented Li-ion batteries have simultaneous functions of energy storage and conversion. A self-charging Li-ion battery that can simultaneously generate and store electric energy by itself could be an important step toward next-generation Li-ion batteries for pushing the practical applications in self-powered electronic devices.

Here, we aim at how to utilize Li-ion batteries to realize energy scavenging for achieving the self-charging functions, where the Li-ion batteries can be easily self-charged up to several volts in a short time. The invented self-charging Li-ion batteries can be utilized to simultaneously scavenge and store ambient mechanical energy from wind blowing. Based on the coupling effect of contact electrification and electrostatic induction, the adjacent electrodes of two Li-ion batteries can generate an output peak voltage of about 200 V and an output peak current of about 25 μA. Flexible Li-ion batteries fabricated by using electrospun $LiMn_2O_4$ nanowires as cathode and carbon nanowires as anode can be charged from 1 to 3.5 V in about 3 min after using a transformer and a rectifier. This research provides a new route for developing next-generation self-charging Li-ion batteries to sustainably power electronics.

Both the anode electrode materials were fabricated by using a facile electrospinning method. **Figure 1**a displays the morphology of the $LiMn_2O_4$ precursor nanowires synthesized by electrospinning before annealing. The nanowires exhibit smooth surfaces with diameters ranging from 150 to 260 nm and lengths of about several tens of micrometers. Figure S1a (Supporting Information) presents the morphology of the annealed $LiMn_2O_4$ precursor nanowires, showing an obvious decrease of the diameters as compared with that of the precursor nanowires. The obtained $LiMn_2O_4$ nanowires as the cathode of Li-ion batteries consist of well-connected $LiMn_2O_4$ nanoparticles with the diameters ranged from 20 to 70 nm, as illustrated in Figure S1b,c (Supporting Information) presents a scanning electron microscope (SEM) image of the obtained

K. Zhao, Prof. Y. Yang, X. Liu, Prof. Z. L. Wang
Beijing Institute of Nanoenergy and Nanosystems
Chinese Academy of Sciences
Beijing 100083, China
E-mail: yayang@binn.cas.cn; zhong.wang@mse.gatech.edu
K. Zhao, Prof. Y. Yang, X. Liu, Prof. Z. L. Wang
CAS Center for Excellence in Nanoscience
National Center for Nanoscience and Technology (NCNST)
Beijing 100190, China
K. Zhao
University of Chinese Academy of Sciences
Beijing 100049, China
Prof. Z. L. Wang
School of Materials Science and Engineering
Georgia Institute of Technology
Atlanta, GA 30332-0245, USA

DOI: 10.1002/aenm.201700103

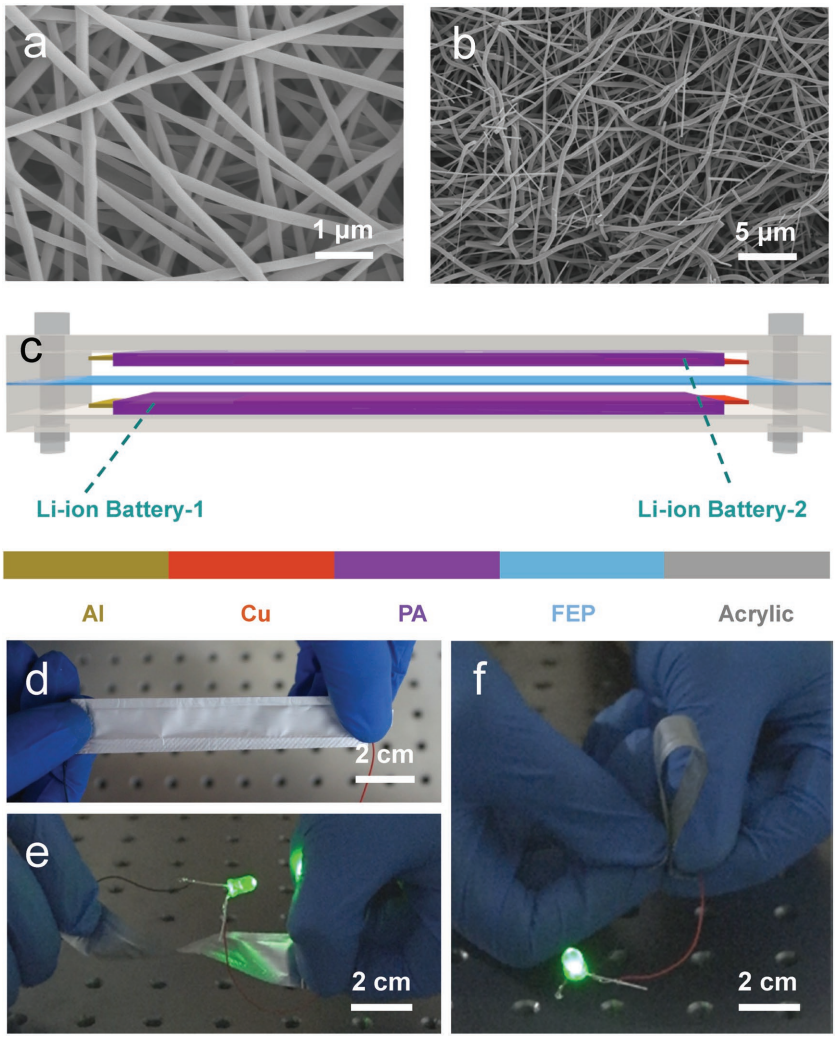

Figure 1. a) SEM image of the $LiMn_2O_4$ precursor nanowires. b) SEM image of the obtained carbon nanowires. c) Schematic diagram of self-charging Li-ion batteries. d) Photograph of a fabricated Li-ion battery. Photographs of the e) twisted and f) bended Li-ion batteries to light up a green LED.

polyvinylpyrrolidone (PVP) nanowires by the electrospinning method, indicating that the PVP nanowires have the diameters of smaller than 650 nm and the lengths of about several tens of micrometers. The PVP nanowires were oxidized under air atmosphere and then was carbonized under Ar protection at 850 °C to form conductive carbon nanowires as the anode of Li-ion batteries, as shown in Figure 1b. Figure S1d (Supporting Information) depicts the X-ray diffraction (XRD) patterns of the obtained $LiMn_2O_4$ and carbon nanowires, where the corresponding diffraction peaks have been calibrated well by using the cubic spinel $LiMn_2O_4$ and C structures, respectively. The as-grown cathode and anode nanowires are important to realize a good cycle stability and high rate capacity due to porous network structures.

As exhibited in Figure 1c, the self-charging Li-ion batteries consist of two flexible Li-ion batteries with two face-to-face cathodes and a hexafluoropropene–tetrafluoroethylene copolymer (FEP) film between two Li-ion batteries, where the two ends of the FEP film was fixed. Figure S2 (Supporting Information) displays photographs of the self-charging Li-ion batteries, where the three parts including two Li-ion batteries and an FEP film can be clearly seen. Figure S3 (Supporting Information) illustrates a schematic diagram of a typical flexible Li-ion battery with 11 different layers. The fabricated Li-ion battery consists of a nano-$LiMn_2O_4$ layer on Al electrode as cathode, a nano-C layer on Cu electrode as anode, and two Al-plastic package layers, which are consistent with the existing flexible commercial Li-ion batteries. Figure 1d presents a photograph of the fabricated flexible Li-ion battery with the dimensions of 100 mm × 18 mm × 0.4 mm. As demonstrated in Figure 1e,f (Movie S1, Supporting Information), a green light emitting diode (LED) can be easily lighted up by the twisted and bended Li-ion batteries after being charged, respectively, indicating that the flexible Li-ion batteries exhibit a good stability under the different mechanical deformations.

Before fabricating the full Li-ion batteries, we measured the performances of the nano-$LiMn_2O_4$ and nano-C layers by using half cells. Figure S4a (Supporting Information) presents the charge and discharge specific capacity–voltage curves of the nano-$LiMn_2O_4$/Li cell at 0.5 C between 2.1 and 4.2 V. Although the corresponding specific capacity exhibits an obvious decrease at the beginning cycles due to the decomposition of electrolyte and formation of the solid electrolyte interphase film on electrode surface, more stable charge and discharge specific capacities can be observed with increasing cycles. Figure S4b (Supporting Information) illustrates the exceedingly stable cycling performance of the nano-$LiMn_2O_4$/Li cell, clearly demonstrating that the charge and discharge specific capacities can be up to about 104.6 and 102.2 mA h g^{-1} at 0.5 C after 200 cycles, respectively. The corresponding coulomb efficiencies are larger than 97%. As displayed in Figure S4c (Supporting Information), the nano-$LiMn_2O_4$ has two similar redox peaks at the first two cycles, suggesting that the polarized sample has a stable structure. Figure S4d (Supporting Information) displays the corresponding rate capability of the nano-$LiMn_2O_4$/Li cell. The specific discharge capacity can be decreased from 130.4 mA h g^{-1} at 0.5 C to 69.2 mA h at 10 C, and then recovered to 123.2 mA h g^{-1} at 0.5 C, indicating that the nano-$LiMn_2O_4$/Li cell has a good rate capability. Figure S4e (Supporting Information) presents the electrochemical impedance spectra of the nano-$LiMn_2O_4$/Li cell, displaying that the nano-$LiMn_2O_4$ has a higher electron conductivity and a lower charge transfer resistance before cycles. However, the slope of the curve after 200 cycles was found to be slightly increased, which is associated with the side reaction product-induced blocking of Li-ion

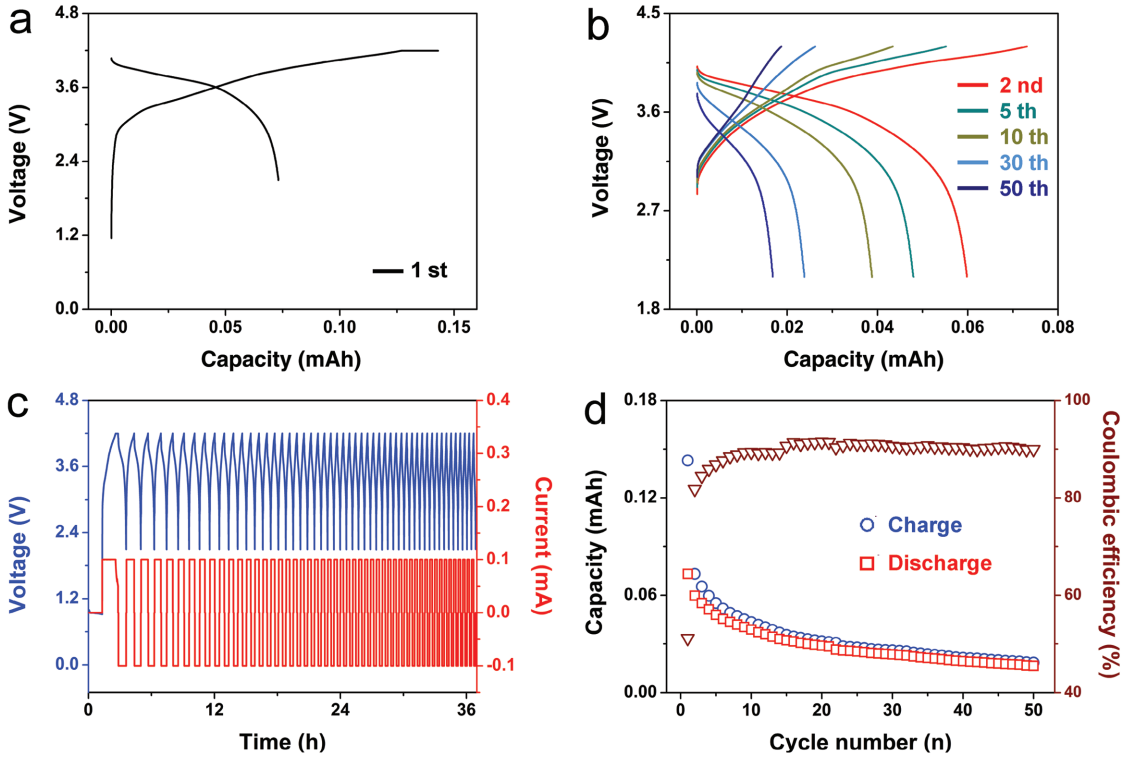

Figure 2. Measured a) 1st and 2nd–50th b) charge/discharge curves of the fabricated Li-ion battery with the voltages ranged from 2.1 to 4.2 V at a current of 0.1 mA. c) Measured charge/discharge voltage–time curves of the Li-ion battery in 50 cycles. d) Charge/discharge capacities and coulombic efficiencies of the Li-ion battery in 50 cycles.

diffusion. Moreover, Figure S5a (Supporting Information) displays the charge and discharge specific capacity–voltage curves of the nano-C/Li cell at 0.5 C between 0 and 3 V. The stable charge and discharge specific capacities can be obtained after 30 cycles, which can be also seen in Figure S5b (Supporting Information). Figure S5c (Supporting Information) presents the cyclic voltammetry (CV) curves of the nano-C/Li cell, where the sharp peaks near 0 V are associated with the insertion of Li-ions into nano-C. The reduction peak at 0.2 V in the initial cycle is due to the decomposition of electrolyte. Owing to the activation of the electrode, the reduction peak has been shifted from 0.2 to 0.6 V in the second cycle. As depicted in Figure S5d (Supporting Information), the nano-C/Li cell has a good rate capability. Figure S5e (Supporting Information) presents the slight decrease of the slope in the electrochemical impedance spectra, which is associated with the increased diffusion rate of the Li-ions in the cycle process to induce the increase of the specific capacity, as illustrated in Figure S5b (Supporting Information).

Figure 2a presents the initial charge and discharge curves of the fabricated flexible Li-ion batteries by utilizing the nano-$LiMn_2O_4$ and nano-C as the cathode and anode, respectively. The charge and discharge capacities in the first cycle are about 143 and 73 μA h, respectively. As displayed in Figure 2b, both the charge and discharge capacities of the Li-ion battery can be decreased with increasing the charge/discharge cycles. Under a constant current of about 0.1 mA, both the charge and discharge voltages of the Li-ion battery were ranged from 2.1 to 4.2 V after the first cycle, as illustrated in Figure 2c. Figure 2d displays the charge–discharge capacities and the corresponding coulombic efficiencies of the Li-ion battery in the 50 cycles, where the charge and discharge capacities are about 18.7 and 16.8 μA h at the 50th cycle, respectively. Although the fabricated Li-ion battery exhibits a low coulombic efficiency of about 51% at the first charge–discharge cycle, the coulombic efficiency can be increased with increasing the charge–discharge cycles to reach a stable value of about 90%, as illustrated in Figure 2d. Figure S6 (Supporting Information) depicts the rate capability of the Li-ion battery, showing that the discharge capacity can be decreased from 23.1 to 5.2 μA h when increasing the current from 0.05 to 0.2 mA. The corresponding discharge capacity can be recovered to 21.9 μA h when the current has been returned to 0.05 mA. Moreover, Figure S7 (Supporting Information) illustrates the charge/discharge capacities and the corresponding coulombic efficiencies of the Li-ion batteries with the electrode overlapping areas of 40 and 200 mm^2, where the charge/discharge capacities values are 11.3/10.2 and 42.6/38.8 μA h at the 100th cycle, respectively. The result indicates that the Li-ion battery capacity is associated with the electrode overlapping areas. To clearly demonstrate the fast self-charging function of the Li-ion battery, the small electrode overlapping area-based Li-ion battery was utilized to effectively store electric energy.

Figure S8 (Supporting Information) illustrates the electricity generation process between two adjacent electrodes of two Li-ion batteries. The coupling between triboelectrification and electrostatic induction can result in the flow of electrons between two electrodes. Here, six different states have been included in the electricity generation process. At the first state, when the FEP film vibrates up to get in touch with the top

Li-ion battery, the same number of negative and positive triboelectric charges can be created on the surfaces of FEP and polyamide (PA) films due to the different triboelectric polarities, respectively. As illustrated in the second state, when the FEP film vibrates down to approach the bottom Li-ion battery, the electrons can flow between two electrodes due to the electrostatic induction. The flow of the electrons can continue until the FEP film gets in touch with the bottom Li-ion battery to reach a new triboelectric charge balance, as exhibited in the third state. After that, the electrons between two electrodes can flow again in a reversed direction as compared with that in the second state. Thus, when the FEP film vibrates between two Li-ion batteries, AC output current/voltage signals between two electrodes can be observed.

Figure 3a,b displays that the output voltage and current between two adjacent electrodes of two Li-ion batteries can be up to about 200 V and 25 μA at a wind speed of about 10 m s^{-1}, respectively. To increase the output current and decrease the output voltage signals for matching the needs of the Li-ion batteries, a transformer has been used to decrease the voltage signals from 200 to 4.7 V and increase the current signals from 25 μA to 0.5 mA, as illustrated in Figure 3c,d, respectively. By measuring the output current signals under different loading resistances, a largest output power can be calculated to be about 1.38 mW under a loading resistance of 6.5 MΩ, as shown in Figure 3e. After using the transformer, the impedance has been decreased to 10 kΩ although the largest output power is about 0.7 mW, as displayed in Figure 3f. The obtained AC output signals can be converted into DC pulse output signals by using a rectifier, as presented in Figure 3g,h. To decrease the secondary reaction of the Li-ion battery, most of the charging voltage signals between two adjacent electrodes after using a transformer and a rectifier are smaller than 4.4 V, as illustrated in Figure 3g. Moreover, previous investigation has indicated that the pulsed voltage/current outputs can induce negligible difference to charge Li-ion batteries as compared with the constant DC signals.[17] We also measured the output voltage signals between two electrodes of only one Li-ion battery under the wind-induced vibrations of the FEP film, as depicted in Figure S9 (Supporting Information). No obvious output voltage signals can be observed although there is a DC output due to the remaining charged voltage of the Li-ion battery.

As illustrated in **Figure 4**a, the self-charging Li-ion batteries consist of two Li-ion batteries and an FEP film, where the two adjacent electrodes of Li-ion batteries were connected to a transformer and then a rectifier for obtaining DC output signals. After that, four switches were utilized to control the connections between the rectifier and the two Li-ion batteries. As shown in Figure 4a, no output current signals can be observed for the energy scavenging unit when the FEP film was in contact with the top Li-ion battery, where both the switches s1 and s2 were closed. When the FEP film was moved down to approach the bottom Li-ion battery, the electrons can flow from the bottom Cu electrode to the top Cu electrode in the energy scavenging unit, as illustrated in Figure 4b. After using the transformer and the rectifier, the produced rectified voltage can result in the outflow of electrons the cathode electrode and the inflow of electrons at the anode electrode at the top Li-ion battery. Under the rectified voltage, the produced Li^+ by the chemical reaction ($LiMn_2O_4 \leftrightarrow Li_{1-x}Mn_2O_4 + xLi^+ + xe^-$) at the cathode electrode can migrate from the cathode electrode to the anode electrode, resulting in the chemical reaction ($6C + xLi^+ + xe^- \leftrightarrow Li_xC_6$) at the anode electrode. When the FEP film was moved up to approach the top Li-ion battery, the top Li-ion battery can be also charged, as displayed in Figure S10 (Supporting Information). Under ambient wind-induced mechanical excitations of the FEP film between the two Li-ion batteries, both the energy scavenging and storage were achieved at the same time, realizing self-charging Li-ion batteries. Moreover, the bottom Li-ion battery can be charged when the switches "s3" and "s4" were turned on and the switches "s1" and "s2" were turned off. Moreover, two Li-ion batteries can provide more electric power to satisfy the requirements of larger electric consumption. When one has no stored electric power, the other one can be switched to ensure the continuous operation of the driving device. As illustrated in Figure 4 and Figure S10 (Supporting Information), the electrons can flow between the two Cu anodes of the two Li-ion batteries when the FEP film vibrates between the two Li-ion batteries, resulting in the AC output signals. There is no energy transfer between the two Li-ion batteries and the driving forces of the electrons movements is due to the FEP film-induced electrostatic induction, resulting in the energy conversion between the mechanical energy and electric energy. As a result, the self-charging process has been achieved by scavenging mechanical energy to charge the corresponding Li-ion battery.

Figure 5a displays the charge–discharge cycling performances of the self-charging Li-ion batteries when the switches 1 and 2 were closed. At the beginning, the top Li-ion battery can be easily charged from 1.5 to 3.5 V in about 3 min under the vibrations of the FEP film induced by a wind blowing at a speed of about 10 m s^{-1} though the device, as presented in Figure 5b. The same self-charging time of about 3 min in the six cycles suggests a good stability of the self-charging Li-ion battery, as displayed in Figure S11 (Supporting Information). After that, the Li-ion battery was discharged under a constant discharging current of 0.1 mA to induce decreased voltages from 3.5 to 1.5 V in about 142 s, where the stored electric capacity was about 3.9 μA h. As compared with the charging/discharging capacities in Figure 2b, the self-charging/discharging capacities are smaller, which is associated with the used less charging time in the self-charging process. To confirm this reason, we fabricated a new device, where the Li-ion battery can be self-charged from 2.1 to 4.2 V under the vibrations of the FEP film, as illustrated in Figure S12a,b (Supporting Information). Under a constant discharging current of 0.1 mA, the Li-ion battery can sustain in about 695 s with the decreased voltages from 4.2 to 2.1 V, resulting in a stored electric capacity of about 19.3 μA h, which is completely consistent with the capacity of the Li-ion battery after 50 cycles (about 20 μA h). Moreover, the Li-ion battery has the same self-charging time of about 11 min in the different six charging cycles (Figure S12c, Supporting Information), indicating that the Li-ion battery has a good stability in the self-charging process. Since the Li-ion battery is in a resting state after being discharged, the retardation of the migration of lithium ions inside the electrode can induce a concentration polarization, resulting in a slow increase for the voltage of the Li-ion battery before charging. After six

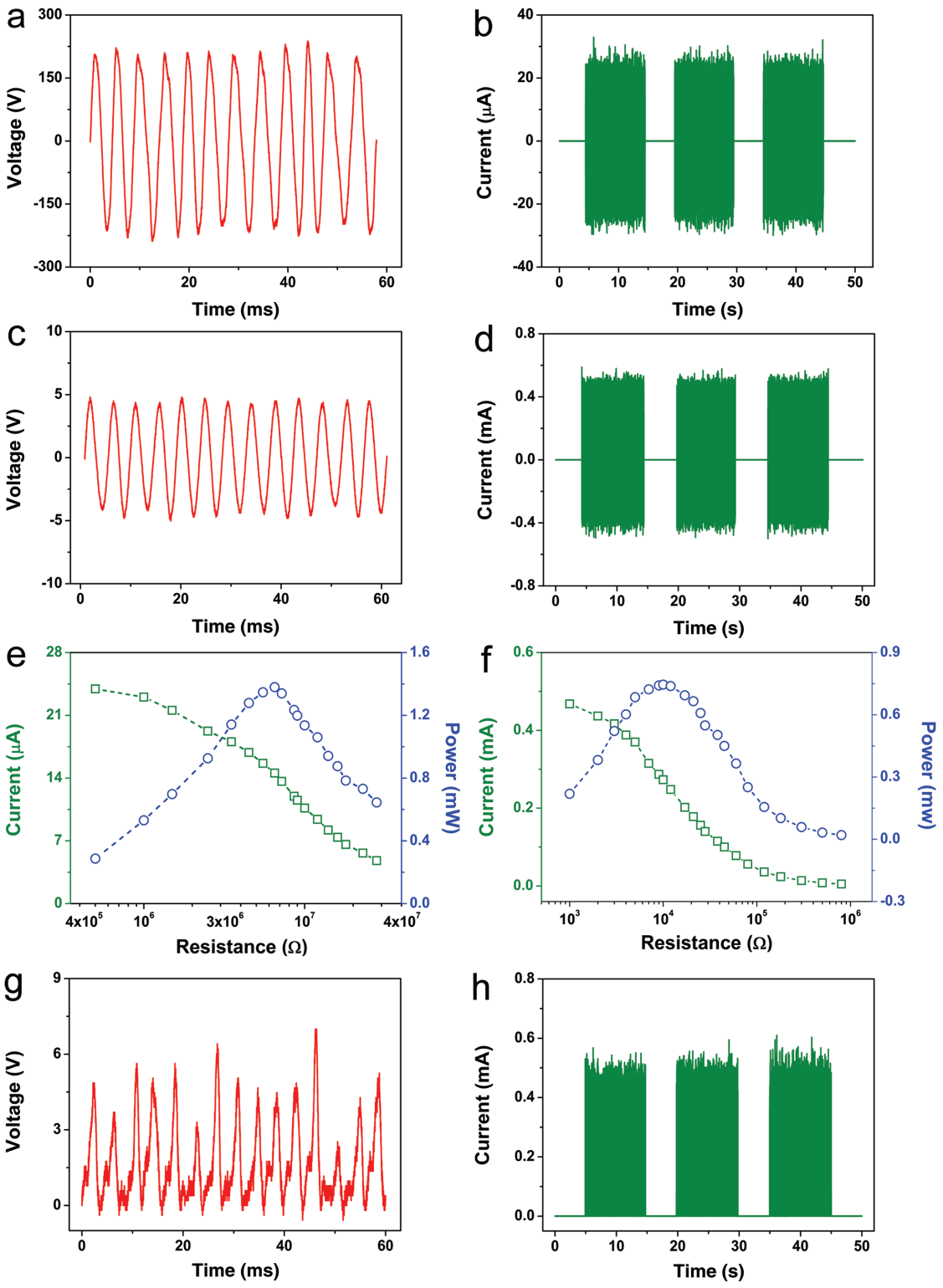

Figure 3. Measured a) output voltage and b) current signals between two adjacent electrodes of two Li-ion batteries. Measured c) output voltage and d) current signals between two adjacent electrodes of two Li-ion batteries after using a transformer. Measured output current signals under the different loading resistances and the corresponding output powers e) before and f) after using a transformer. Measured g) output voltage and h) current signals between two adjacent electrodes of two Li-ion batteries after using a transformer and a rectifier.

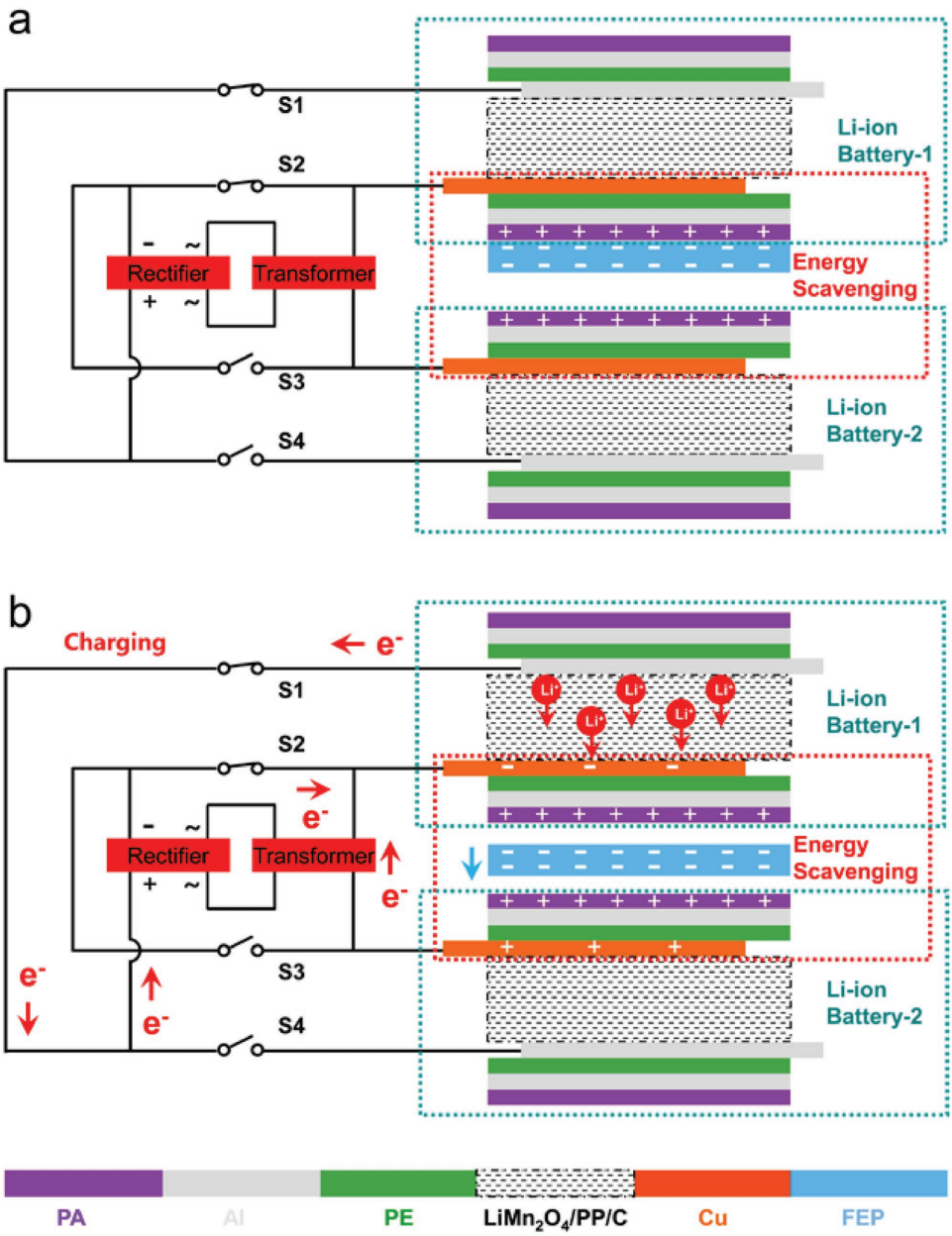

Figure 4. a) Schematic diagram of self-charging process for the Li-ion batteries with no output for the energy scavenging unit. b) Schematic diagram of self-charging process for the Li-ion batteries, clearly showing the flow of electrons in the circuit.

charge–discharge cycles, we measured the voltage of the Li-ion battery in about 30 min without the working of the energy scavenging unit as a control experiment, exhibiting that the voltage of the Li-ion battery was maintained at a stable value of about 1.2 V, as illustrated in Figure 5a. Figure S13a (Supporting Information) depicts the charge–discharge cycling performances of the self-charging Li-ion batteries when the switches 3 and 4 were closed, clearly indicating that the bottom Li-ion battery can be also effectively charged by wind-induced working of the energy scavenging unit in the self-charging batteries. Figure S13b (Supporting Information) displays the enlarged charge–discharge curve of the bottom Li-ion battery, showing a clear charging and discharging processes as compared with that of no charging process in Figure S13a (Supporting Information) after 120 s.

We also measured the stability of the electrochemical performances of Li-ion batteries when the energy scavenging unit was working due to wind induced vibration of the FEP film. Figure S14 (Supporting Information) illustrates the charge and discharge curves of an Li-ion battery with no wind induced vibration of the FEP film in the first 20 cycles. The detailed charge and discharge voltages of a new Li-ion battery in the 50 cycles are presented in Figure 5c, showing that no obvious difference can be observed with and without the wind-induced vibration of the FEP film. Figure 5d displays the charge–discharge capacities and the corresponding coulombic efficiencies of a new Li-ion

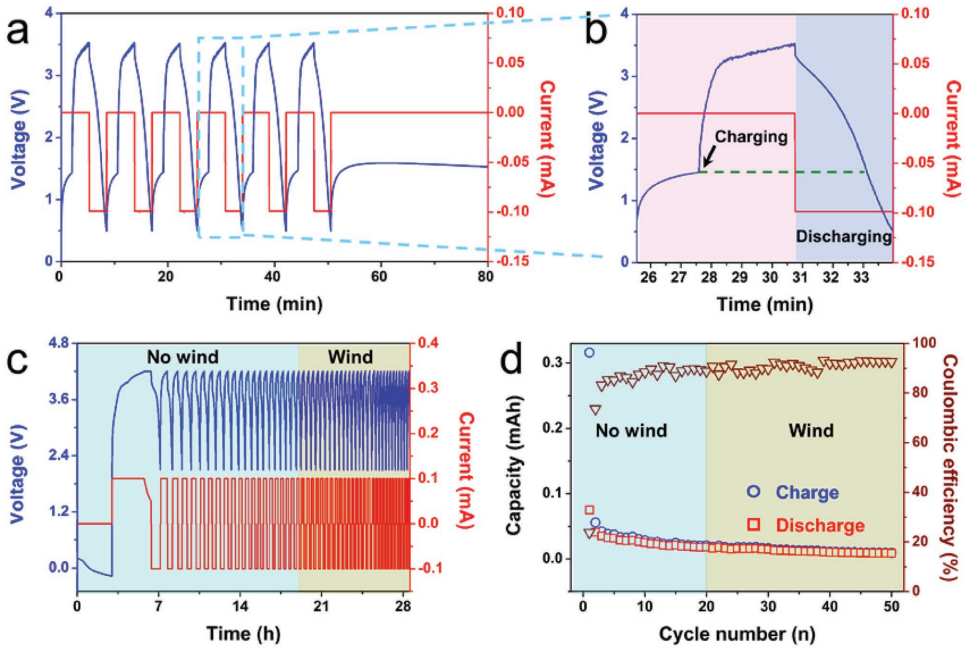

Figure 5. a,b) Self-charging and discharging curves of the top Li-ion battery, where the enlarged curve is shown in (b) under a discharge current of about 0.1 mA. c) Measured charge/discharge voltage–time curves of a new Li-ion battery in 50 cycles with no wind through the device in the first 20 cycles. d) Charge/discharge capacities and coulombic efficiencies of a new Li-ion battery in 50 cycles with no wind through the device in the first 20 cycles.

battery in the 50 cycles, indicating that the Li-ion battery has stable electrochemical performances with and without the wind induced vibrations of the FEP film. Figure S15 (Supporting Information) depicts the charge and discharge capacities of different six Li-ion batteries under the conditions of with and without the wind induced vibrations of the FEP film. All the six Li-ion batteries have the similar change tendencies, where the working of the energy scavenging unit has no obvious effect on the electrochemical performances of the Li-ion batteries. As illustrated in Figure S15 (Supporting Information), although the capacity of the Li-ion battery exhibits obvious decrease in the first 40 cycles, the corresponding capacity becomes more and more stable after 40 cycles, as depicted in Figure S13b,d (Supporting Information). In this study, all self-charging performances of the Li-ion batteries were measured after 50 cycles. When the mechanical inputs are more random, less electric energy generated from the system due to possible lower wind speeds can result in the increase of self-charging time. However, the designed self-charging Li-ion batteries still can be self-operated under random mechanical inputs since the random mechanical stimuli also can induce sustainable working of the energy scavenging unit in the system.

In summary, we have developed self-charging Li-ion batteries to simultaneously scavenge and store mechanical energy. Based on the electrospun $LiMn_2O_4$ nanowires as cathode and carbon nanowires as anode, the fabricated flexible Li-ion batteries exhibit a capacity retention of 90% coulombic efficiency after 50 cycles. The adjacent electrodes of two Li-ion batteries can deliver an output peak voltage of about 200 V and an output peak current of about 25 μA by using the coupling between triboelectrification and electrostatic induction. Under ambient wind-induced mechanical excitations of an FEP film between the two Li-ion batteries, the self-charging Li-ion batteries can easily charge themselves up to 3.5 V in about 3 min. This research demonstrates the feasibility of utilizing Li-ion batteries as both the energy storage and scavenging units for the potential applications in sustainably powering electronic devices and self-powered systems.

Experimental Section

Preparation of $LiMn_2O_4$ Nanowires: PVP ($M_w \approx 1\,300\,000$) of 8.4 g was dissolved 47.8 g ethanol under a constant stirring for 8 h. After that, for $LiMn_2O_4$ precursor, lithium acetate ($Li(CH_3COO)$) and manganese (II) nitrate tetrahydrate ($Mn(NO_3)_2{\cdot}4H_2O$) with a stoichiometric ratio of 1:2 and the total mass of 4.5 g was dissolved in 33 g demonized water. The PVP-ethanol solution and $LiMn_2O_4$ precursor aqueous solution (PVP-ethanol solution and $LiMn_2O_4$ precursor aqueous solution with mass ratio in 1.5:1) were mixed and stirred for 16 h. The mixed solution was delivered in 20 mL plastic syringe which was connected by a stainless steel needle. A positive voltage of 21.79 kV and a negative voltage of −1.86 kV were applied between the metal needle tip and an aluminum foil collector with a distance of 10 cm. The polymer jet was ejected at a constant flow rate of 0.08 mm min^{-1}. $LiMn_2O_4$ nanowires as the cathode material were obtained by annealing the precursor nanowires at 500 °C for 1 h and 600 °C for 5 h in air at the heating rate of 5 °C min^{-1} and then cooling to room temperature in the muffle furnace.

Preparation of Carbon Nanowires: PVP nanowires were also prepared by using an electrospinning technique. The spinning solution was obtained by mixing 9 g of PVP in 91 g ethanol under constant stirring for 8 h. A positive voltage of 11.68 kV and a negative voltage of −1.86 kV were set between the metal needle tip and an aluminum foil collector. A flow rate of 0.06 mm min^{-1} was kept. Carbon nanowires were obtained by preoxidizing the PVP nanowires at 150 °C for 24 h, 280 °C for 2 h in air and carbonizing the preoxidized nanowires at 750 °C for 2 h in high purity N_2 at a heating rate of 5 °C min^{-1} and then cooling to room temperature in the tube furnace.

Fabrication of the Li-Ion Battery: The working electrodes of the Li-ion battery were fabricated by mixing the active material, acetylene black, and PVP with the weight ratio of 8:1:1 in deionized water to obtain slurries. The as-prepared cathode and anode slurries were coated on Al foil and Cu foil, respectively. The coating thickness is about 100 µm. Then, electrodes were dried in a vacuum-drying oven at 110 °C for 24 h and then were cut into rectangle electrodes (90 mm × 4 mm). Flexible Li-ion batteries were assembled in an argon-filled glove box. A flexible Al-plastic composite film (PA/Al/Polyethylene, 100 mm × 18 mm × 0.09 mm) was utilized for the package, a porous polypropylene film as separator, and the solution of 1 mol L^{-1} $LiPF_6$ in ethylene carbonate/ethyl methyl carbonate with the volume ratio 1:1 as electrolyte.

Fabrication of the Self-Charging Li-Ion Batteries: The fabricated self-charging Li-ion batteries consist of an FEP film and two Li-ion batteries. The working mechanism of power generation is based on the wind-induced vibration of the FEP film to realize the periodic vibration and separation between FEP film and the two Li-ion batteries. Two acrylic plates (130 mm × 18 mm × 3 mm) as the substrates were cut by using a laser cutting machine. Two holes with a diameter of 5 mm were fabricated at both ends of the acrylic sheets. The supporting beams (18 mm × 10 mm × 1.2 mm) were fixed between two acrylic sheets. Screws were used to fix the two ends of the FEP film (130 mm × 18 mm × 0.04 mm) in the middle of the device. When the wind flowed into the device, the FEP film can vibrate up and down to contact the PA layer of the Al-plastic composite film of Li-ion battery surface, resulting in the observed output voltage/current signals.

Characterizations and Measurements: The morphology of the nanowires was characterized using a field-emission scanning electron microscope (SU8020). The crystal structure was identified by XRD, which using Cu *Kα* radiation. The button cells were assembled in a glove box using Li plate as the anode. The electrochemical properties of the Li-ion batteries were tested using an MTI eight channels battery analyzer (CT-3008-5 V and 1 mA, CT-3008W-5 V and 10 mA). Electrochemical impedance spectroscopy and CV were performed using an electrochemical workstation (Versa STAT 4). The output voltage and current signals of the self-charging Li-ion batteries were measured by a mixed domain oscilloscope (Tektronix MDO3024) and a low-noise current preamplifier (Stanford Research SR570), respectively.

Supporting Information

Supporting Information is available from the Wiley Online Library or from the author.

Acknowledgements

This work was supported by the National Natural Science Foundation of China (Grant Nos. 51472055 and 61404034), External Cooperation Program of BIC, Chinese Academy of Sciences (Grant No. 121411KYS820150028), the 2015 Annual Beijing Talents Fund (Grant No. 2015000021223ZK32), the National Key R&D Project from Minister of Science and Technology in China (Grant Nos. 2016YFA0202701 and 2016YFA0202704), and the "thousands talents" program for the pioneer researcher and his innovation team, China. The corresponding patent based on this work presented here has been submitted.

Conflict of Interest

The authors declare no conflict of interest.

Keywords

Li-ion batteries, $LiMn_2O_4$ nanowires, self-charging, triboelectrification, wind energy

Received: January 11, 2017
Revised: June 6, 2017
Published online:

[1] A. S. Arico, P. Bruce, B. Scrosati, J. M. Tarascon, W. Van Schalkwijk, *Nat. Mater.* **2005**, *4*, 366.
[2] Z. L. Wang, *Adv. Funct. Mater.* **2008**, *18*, 3553.
[3] N. J. Dudney, J. Li, *Science* **2015**, *347*, 131.
[4] Y. Sun, N. Liu, Y. Cui, *Nat. Energy* **2016**, *1*, 16071.
[5] M. Ko, S. Chae, J. Ma, N. Kim, H.-W. Lee, Y. Cui, J. Cho, *Nat. Energy* **2016**, *1*, 16113.
[6] Y. Liu, D. Lin, Z. Liang, J. Zhao, K. Yan, Y. Cui, *Nat. Commun.* **2016**, *7*, 10992.
[7] N. J. Jeon, J. H. Noh, W. S. Yang, Y. C. Kim, S. Ryu, J. Seo, S. I. Seok, *Nature* **2015**, *517*, 476.
[8] L.-D. Zhao, S.-H. Lo, Y. Zhang, H. Sun, G. Tan, C. Uher, C. Wolverton, V. P. Dravid, M. G. Kanatzidis, *Nature* **2014**, *508*, 373.
[9] Y. Yang, W. Guo, K. C. Pradel, G. Zhu, Y. S. Zhou, Y. Zhang, Y. Hu, L. Lin, Z. L. Wang, *Nano Lett.* **2012**, *12*, 2833.
[10] W. Wu, L. Wang, Y. Li, F. Zhang, L. Lin, S. Niu, D. Chenet, X. Zhang, Y. Hao, T. F. Heinz, J. Hone, Z. L. Wang, *Nature* **2014**, *514*, 470.
[11] Z. L. Wang, J. Song, *Science* **2006**, *312*, 242.
[12] J. Chun, B. U. Ye, J. W. Lee, D. Choi, C.-Y. Kang, S.-W. Kim, Z. L. Wang, J. M. Baik, *Nat. Commun.* **2016**, *7*, 12985.
[13] Y. Yang, Y. S. Zhou, H. Zhang, Y. Liu, S. Lee, Z. L. Wang, *Adv. Mater.* **2013**, *25*, 6594.
[14] S. Wang, X. Mu, Y. Yang, C. Sun, A. Y. Gu, Z. L. Wang, *Adv. Mater.* **2015**, *27*, 240.
[15] H. Guo, J. Chen, L. Tian, Q. Leng, Y. Xi, C. Hu, *ACS Appl. Mater. Inter.* **2014**, *6*, 17184.
[16] T. Kim, J. Chung, D. Y. Kim, J. H. Moon, S. Lee, M. Cho, S. H. Lee, S. Lee, *Nano Energy* **2016**, *27*, 340.
[17] X. Pu, M. Liu, L. Li, C. Zhang, Y. Pang, C. Jiang, L. Shao, W. Hu, Z. L. Wang, *Adv. Sci.* **2016**, *3*, 1500255.